

Remote Visual Analysis of Large Turbulence Databases at Multiple Scales

Jesus Pulido^{a,b,*}, Daniel Livescu^b, Kalin Kanov^c, Randal Burns^c, Curtis Canada^b, James Ahrens^b, Bernd Hamann^a

^a*Department of Computer Science, University of California, Davis, CA 95616, USA*

^b*Los Alamos National Laboratory, Los Alamos, NM 87544, USA*

^c*Johns Hopkins University, Baltimore, MD 21218, USA*

Abstract

The remote analysis and visualization of raw large turbulence datasets is challenging. Current accurate direct numerical simulations (DNS) of turbulent flows generate datasets with billions of points per time-step and several thousand time-steps per simulation. Until recently, the analysis and visualization of such datasets was restricted to scientists with access to large supercomputers. The public Johns Hopkins Turbulence database simplifies access to multi-terabyte turbulence datasets and facilitates the computation of statistics and extraction of features through the use of commodity hardware. We present a framework designed around wavelet-based compression for high-speed visualization of large datasets and methods supporting multi-resolution analysis of turbulence. By integrating common technologies, this framework enables remote access to tools available on supercomputers and over 230 terabytes of DNS data over the Web. The database toolset is expanded by providing access to exploratory data analysis tools, such as wavelet decomposition capabilities and coherent feature extraction.

Keywords: Databases, Wavelets, Data Reduction, Remote Visualization, Distributed Systems, Turbulence

*Corresponding author

Email addresses: jpulido@ucdavis.edu, Ph.+1 (209) 261-2674 (Jesus Pulido), livescu@lanl.gov (Daniel Livescu), kalin@cs.jhu.edu (Kalin Kanov), randal@cs.jhu.edu (Randal Burns), cvc@lanl.gov (Curtis Canada), ahrens@lanl.gov (James Ahrens), hamann@cs.ucdavis.edu (Bernd Hamann)

1. Introduction

Extremely large datasets commonly arise in science and engineering today, and it is often prohibitive to store an original massive dataset at multiple sites or transmit it over computer networks in its entirety. Regardless, such datasets represented tremendous scientific value for the broader scientific community. It is imperative to deploy effective technologies enabling the remote access to vast data archives for the purpose of having a large pool of scientists harness their value and make new discoveries. Our analysis framework presented here was driven specifically by the needs articulated by scientists from Johns Hopkins University (JHU) and Los Alamos National Laboratory. JHU hosts a large digital repository of data from several disciplines, including massive simulation data from numerical simulations of turbulent physics. The framework we present makes remote visual analysis possible via an effective protocol controlling the distribution of analysis and visualization steps to be performed on the server side (JHU site) and a remotely connected visualization client.

Furthermore, our framework incorporates the power of approximating a dataset by using cubic (bi-cubic, tri-cubic) B-spline wavelets. The utilization of wavelet approximation allows a user to generate initial previews or simply coarse approximations of a dataset quickly, making possible the efficient identification of specific regions of interest that might warrant an analysis at a more detailed level. We demonstrate our framework for datasets available in the JHU repository and for typical scientific analysis scenarios.

Most datasets encountered in applications in the physical sciences, similar to most natural images, present lower-dimensional structures whose detection, extraction, and characterization are active areas of research. The search for more efficient algorithms to detect and manipulate such structures has led to the development of a multitude of multi-resolution geometric methods supporting data analysis at multiple scales. One area that significant benefits from the application of such methods is fluid turbulence. In general, turbulent flows contain localized, highly intermittent structures as well as more stable, coherent structures. The characterization of these structures, which interact nonlinearly as they are advected by the background flow and significantly alter the local topology, is an open, fundamental question in the study of turbulence. Multi-resolution rep-

29 representation methods seem ideally suited for such an effort due to their localization in both the real
30 and frequency spaces.

31 Recently, Pulido et al. [1], studied several multi-resolution representation methods in depth,
32 including B-spline, Daubechies and Coiflet wavelets, curvelets and surfacelets. These methods
33 were compared to determine their ability to capture the structure of fully developed turbulence
34 using a truncated set of coefficients. Methods were evaluated based on their ability to approximate
35 scalar and vector fields, including density and velocity, as well as derived data such as derivatives,
36 spectra, and properties of constant density surfaces. The main criteria used for comparing meth-
37 ods were computational efficiency, numerical accuracy, and degree of data compression. While
38 different methods performed better with respect to various metrics, B-spline wavelets consistently
39 ranked at or near the top of the metrics considered. Except for some of the orthogonal wavelet
40 methods, the use of multi-resolution representation techniques to study turbulence is relatively
41 new and an emerging area of research. In particular, the B-spline wavelets have only been sparsely
42 used for such purpose. Here, we present the addition of the B-spline wavelet representation to the
43 JHU turbulence database. By overcoming bottlenecks in the system, we demonstrate this tool for
44 both remote visualization and novel multi-scale analysis of turbulence data.

45 *1.1. Contributions*

46 This paper contains the following contributions:

- 47 • Wavelet compression is introduced at the data-level to reduce access costs, bandwidth, mem-
48 ory and compute footprint, therefore improving latency between database components to
49 support many remote users.
- 50 • Remote visualization is made possible for a multi-terabyte database cluster supporting com-
51 modity hardware.
- 52 • New analysis tools are demonstrated for two datasets for these types of turbulence: a) Homo-
53 geneous Buoyancy Driven Turbulence (HBDT) [2] and b) Forced Magneto-Hydrodynamic
54 turbulence (FMHDT) [3].

55 In Sections 2 and 3, we discuss related works in remote visualization and wavelet compression,
56 describe the public JHU database cluster, and provide a brief introduction to wavelet methods.
57 Section 4 presents a pipeline that introduces wavelet methods and visualization support to the
58 JHU database cluster. Section 5 discusses results focused on measures assessing the performance,
59 quality, and efficiency of using wavelet methods for analysis. Additionally, multi-scale analysis
60 is performed, driven by domain scientists, and results are presented using the newly implemented
61 analysis tools. Our conclusions in Section 6 summarize our results and contributions.

62 **2. Related Work**

63 With the continued and rapid growth of the size of datasets, movement of data is increasingly
64 difficult. Database systems, such as the Johns Hopkins Turbulence Database (JHTDB) [4], pro-
65 vide public access via Web services to large datasets in a database cluster. Efficient and remote
66 Visualization and analysis capabilities are crucially important for understanding such large-scale
67 simulated datasets, to gain the desired value and scientific insight from the available data.

68 Compression for reducing bottleneck behavior in systems for data visualization purposes has
69 been explored previously. Classic methods, such as Haar wavelets, are used in Computational
70 Fluid Dynamics (CFD) for data transmission in Trott et al. [5]. Lippert et al. [6] applied wavelet
71 splats, permitting lossy compression, to enable volume rendering of large datasets. Concern-
72 ing large-scale and remote data visualization, Guthe et al. [7] proposed the use of hierarchical
73 wavelets in a preprocessing step to reduce hardware requirements for volume visualization ap-
74 plications. While this technique reduces the cost of visualization on standard PCs, interactive
75 data walkthrough leads to rendering times exceeding 1000ms per frame, unless wavelet coeffi-
76 cients are cached. Woodring et al. [8] used a commercial wavelet standard, Jpeg2000, to perform
77 compression over the network. Lakshminarasimhan et al. [9] described a new error-bound, B-
78 spline-fitting-based method for lossy data compression and performed a direct comparison with
79 wavelets. When comparing the method to traditional Haar and other linear wavelet methods, it has
80 been shown to perform rather poorly for data analysis and visualization purposes [1]. Lindstrom et
81 al. [10] developed a fixed-rate, near-lossless compression scheme targeting floating-point gridded
82 data. While these compression schemes are useful for data storage purposes and transfer over net-

83 works, they do not enable the analysis of data for a band-/frequency-specific analysis, which is of
84 great interest in the context of a scale-based analysis of phenomena exhibiting behavior at multiple
85 scales. In our framework, we use cubic B-spline wavelets that significantly improve over linear
86 wavelets, then only stream the coefficients required for a specific scale, without decompression.
87 This approach supports fast adaptive refinement of coefficients to improve the level of detail of an
88 approximation when requested.

89 Several visualization frameworks and systems have been developed over the past years. Ahrens
90 et al. [11] devised Paraview, which is the underlying system we used for our efforts discussed in
91 this paper. Childs et al. [12] developed another system, called Visit. Both systems are built on
92 the Visualization Tool Kit (VTK) [13] and provide a most of the commonly used and needed data
93 visualization methods. Cedilnik et al. [14] presented several remote visualization schemes and
94 implemented them in Paraview. These schemes are based on streaming compressed images and
95 geometrical data over a network, but they do not address the problem of processing large amounts
96 of data at the location where the data physically reside. In our framework, we compress data at
97 the database level and augment existing features of Paraview, including decompression capability
98 to represent reduced datasets supporting concurrent users in a single node.

99 Finally, [15] provides an overview of visualization of large turbulence datasets, proposing the
100 use of a GPU-based wavelet methods for data compression. Local large data can be processed
101 quickly on a Desktop client's GPU by using a bricking scheme that reduces workloads into smaller
102 compute blocks. Remote visualization, however, has to contend with the existing server limitations
103 as it is not feasible to transfer all the data locally. Additionally, the existing JHTDB framework is
104 limited by monetary cost to the usage of headless nodes without a GPU. Our wavelet approach is
105 CPU-based by design, and many times does not require a full wavelet computation of the domain.
106 If a user requests a subset of a dataset, only that portion is compressed and cached rather than the
107 entire domain as does a comparable bricking scheme. Once computed or recalled from cache, we
108 can directly visualize the raw, compressed coefficients without the need of a full decompression
109 (reconstruction) of the data. With this process, our approach greatly reduces processing require-
110 ments for scientific discovery as it allows multiple users to explore datasets in a single node. The
111 bricking scheme proposed in [15] may still be useful for future larger datasets, as they become

112 memory bound.

113 Several elegant techniques for the analysis of turbulent CFD datasets were recently developed.
114 For example, Roussel et al. [16] discussed the use of biorthogonal (constant) Harten wavelets for
115 the extraction of coherent vortices and found that biorthogonal wavelets can cause problems when
116 modeling background noise after feature extraction. Laney et al. [17] developed an approach for
117 analyzing Rayleigh-Taylor instabilities using the Morse complex and visualizing features based
118 on it. Finally, Bremer et al. [18] introduced a method that employs a hierarchical segmenta-
119 tion method to analyze and track isosurfaces in time-dependent datasets. While computationally
120 expensive for large datasets, the flexibility offered by our framework makes it possible the imple-
121 mentation for feature-sets beyond that of the JHTDB, for reduced sets, or for datasets with high
122 temporal fidelity.

123 **3. Background**

124 In this section, we give an overview of a public database framework and architecture available
125 for remote data analysis. This section also introduces the wavelet techniques used for the proposed
126 architecture.

127 Accurate simulations of turbulent flows require solving all the dynamically relevant scales of
128 motions. This technique is usually referred to as direct numerical simulation (DNS). Since tur-
129 bulence is a strongly multi-scale phenomenon with a large range of dynamically relevant spatio-
130 temporal scales, such computations are restricted to relatively simple flows and require the use
131 of the largest supercomputers available. The pace and scale at which such simulations are per-
132 formed only continues to increase; consequently, the simulations themselves are restricted to a
133 small number of groups worldwide with access to large computational platforms. In addition, the
134 large databases generated make the analysis, visualization and sharing of the results extremely
135 challenging in their own rights. Even transferring the data resulting from these simulations from
136 archive systems to the local scratch for further post processing is becoming very time consum-
137 ing. Yet the petabytes of turbulence data, spanning a rapidly increasing range of flows, each with
138 many different parameters, offer almost limitless information on many different aspects of the flow,
139 from an infinite mathematically) hierarchy of turbulence moments and their Probability Density

140 Functions (PDF), spectra, and correlations, to structure-functions, geometrical properties, etc. The
 141 ability to share such datasets with other groups in the open science community can significantly
 142 reduce the time to analyze the data (currently measured in years), help the creative process and in-
 143 crease the pace of discovery and, ultimately, advance our knowledge and ability to model turbulent
 144 flows.

145 3.1. Johns Hopkins Turbulence Database

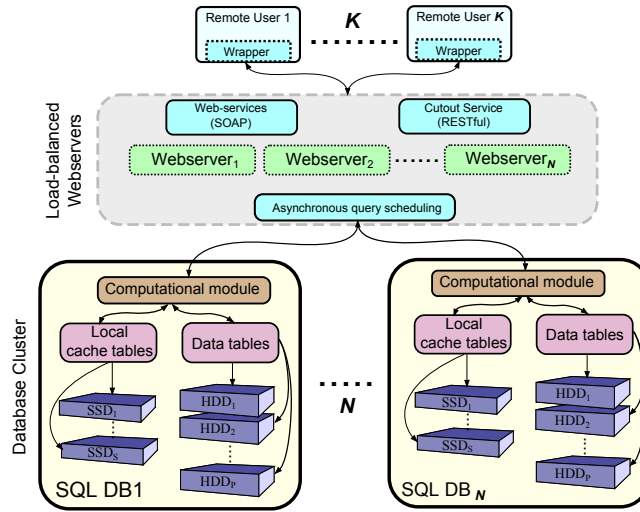


Figure 1: Architecture overview of the JHTDB. Multiple N server nodes create a database cluster to serve K users. The web services module provides an API where remote users may place requests to the database.

146 The Johns Hopkins Turbulence Database (JHTDB) is a public database system used for storing
 147 DNS datasets. Unlike other public databases, JHTDB also provides several remote tools that fa-
 148 cilitate the analysis and retrieval of turbulence data [4]. The DNS datasets available are: a) forced
 149 isotropic turbulence, b) incompressible magnetohydrodynamic (MHD) turbulence [3], c) forced,
 150 fully developed turbulent channel flow [19], and d) homogeneous buoyancy driven turbulence [2].
 151 The datasets consist of files with the values of the primary variables (e.g. velocity vector com-
 152 ponents, density, pressure etc.) specified at 1024^3 spatial points and multiple time-samples (up to
 153 1024). Planned for the future are datasets as large as 4096^3 . The complete space-time history of
 154 turbulence is currently accessible to users remotely through an interface that is based on a Web-

155 services model. Users may write and execute analysis programs on their host computers, while the
156 programs make calls that request desired parts of the data over the network. Users now are able
157 to remotely calculate various statistical data by accessing the 230 Terabytes of DNS data using
158 regular platforms such as laptops. Fig. 1 gives a brief overview of the JHTDB architecture used to
159 support a database. Data are partitioned spatially and temporally across the cluster and accessed
160 through a database access server hosting a Web services module. This module allows for schedul-
161 ing and divides user requests to according to the partitioning of the data. Remote users interact
162 with the database through SOAP and RESTful web protocols via wrappers in multiple languages
163 such as Matlab, Python, C and Fortran.

164 The architecture of the database is explained in detail, including descriptions for locally defined
165 functions such as differentiation and interpolation, by Li et al. [20]. In this paper, test calculations
166 are performed to illustrate the usage of the system and to verify the accuracy of the methods
167 in a parallel environment. The database is then used to analyze a dynamical model for small-
168 scale intermittency in turbulence to show that these effects differ considerably among themselves
169 and thus require different modeling strategies in Lagrangian models of velocity increments and
170 intermittency.

171 Although a variety of remote analysis tools are publicly available through this cluster, there
172 is currently no support for scalable remote visualization. In addition, the tools we have added to
173 enable such support can also be used for novel turbulence analysis, including scale decomposition
174 and coherent feature extraction.

175 *3.2. B-splines and Wavelets*

176 Wavelets are the generalization of the Fourier transform by using bases that represent both
177 location and spatial frequency [21]. Previously, Farge [22] performed an initial analysis on the use
178 of wavelets, for turbulence to characterize coherent and incoherent flow parts.

179 In a more recent effort by Pulido et al. [1], several multi-resolution representation methods
180 were compared, including higher-order B-spline wavelets, for their ability to capture a broad range
181 of quantities pertaining to the turbulence structure with a reduced set of coefficients. Biorthogonal
182 B-spline wavelets have compact support and the added advantage that their bases functions can be

183 specified analytically. The wavelets used in this analysis are mostly second-generation wavelets in
184 implementation [23].

185 After a detailed analysis of multiple wavelets, Pulido et al. [1] showed that the higher-order
186 B-spline families consistently ranked amongst the top for the metrics considered. Wavelets of
187 lower-order (first, second) were not able to represent an original or derivative signal well and a
188 wavelet of too high-order (sixth, seventh) introduced oscillations into the data. Based on this work,
189 we selected cubic B-spline wavelets due to their overall very good performance for compression
190 and analysis. By considering a sinusoidal signal instead of a typical binary, a wavelet transform is
191 able to capture superior directionality of a dataset. Nevertheless, the wavelet framework presented
192 in this paper has support for many other wavelet degrees and families such as Daubechies. The
193 discrete versions of these signals are used in form of filters as described by [24].

194 **4. Method**

195 The ability to efficiently explore the large datasets stored in the JHTDB require that remote data
196 exploration and visualization techniques are supported by proper multi-resolution technology. For
197 this purpose, we decided to integrate wavelet methods as a module that is tightly integrated with
198 the database cluster itself. Our integrated wavelet module supports the efficient decomposition
199 and reconstruction algorithms needed for the requirements of a remote, real-time-driven data ex-
200 ploration framework using long-distance computer networks. Our wavelet implementation further
201 supports various ways to effectively select and combine those coefficients of a wavelet decompo-
202 sition that enable data-specific and user-specific reconstruction of data, emphasizing, for example,
203 frequency and band-specific utilization of coefficients for data analysis. In summary, our coupling
204 of wavelet technology and the JHTDB now make it possible to browse massive datasets much
205 more efficiently than before, thereby greatly increasing the pool of scientific users of the JHTDB.

206 The following section describes the current and augmented pipeline proposed in this paper. A
207 diagram with the high-level structure of the system can be seen in Fig. 2. There are two primary
208 augmentations made to the existing pipeline. The first is the addition of wavelet support to the
209 database cluster as a computational module. The second is the addition of a new type of node, a

210 visualization node that hosts a visualization server and directly communicates with the database
 211 cluster.

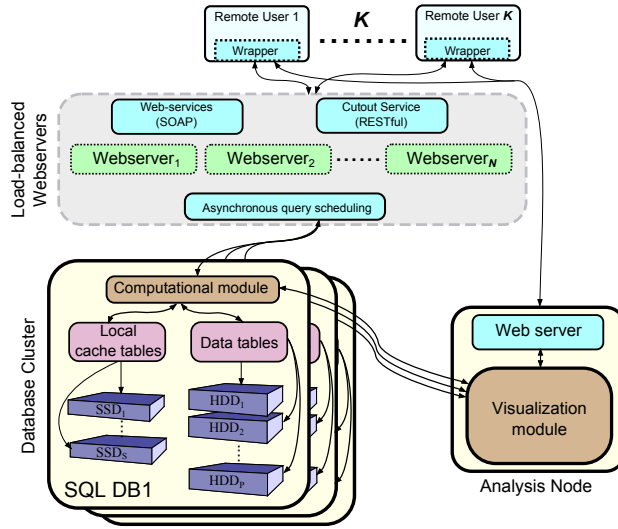


Figure 2: Updated architecture overview for the JHTDB. With wavelet support implemented on both the database cluster and the analysis node, many concurrent users are able to visualize stored datasets using the JHTDB and a visualization node with commodity hardware.

212 *4.1. Wavelet Integration*

213 Wavelet support is added directly to the existing compute capabilities of the JHTDB. Designed
 214 as a new database cluster’s computational module, wavelet decomposition, reconstruction, and
 215 coefficient manipulation capabilities are added to the cluster itself and to the proposed visualization
 216 module.

217 The wavelet CPU implementation is based on the GNU Scientific Library (GSL) [25]. A
 218 large number of modifications were made to the open source library. We enabled support for 3D
 219 wavelet decomposition, higher-order B-spline basis functions, border effects, support for odd and
 220 non-power-of-two-resolution datasets, and parallel computation. Since the wavelets available in
 221 the GSL are discrete, filter-based, it is possible to consider additional discrete wavelets to be added
 222 to existing ones.

223 A wavelet operation (decomposition) is typically carried out when a dataset is first requested,
224 prompting the computation of the wavelet coefficients of the entire dataset. Coefficients are cached
225 for future requests of the same dataset. Once the coefficients are computed, there are several
226 distinct methods for manipulating the coefficients involving the selection of specific or a series of
227 coefficients. This selection is typically known as hard thresholding. Unnecessary coefficients do
228 not need to be sent over the network. The thresholding process is a linear operation that can be
229 performed efficiently. Several thresholding methods exist that allow a user to construct and explore
230 a reconstruction, or a specific feature-set of a large dataset. Some of these methods are included
231 as available options and described below.

232 A key benefit of using wavelets for data reduction rather than sampling data at lower resolutions
233 is their ability to refine lower-resolution data representations into higher quality with low effort.
234 The first and default method of coefficient selection involves the preservation of coefficients up to
235 a certain scale. When supporting many concurrent users accessing data and performing analysis
236 over a network, this method is used to reduce bandwidth to the visualization node and memory
237 requirements. This selection results in data compressed up to several resolutions at varying quality
238 levels, where larger-scale, dominant features are preserved at the loss of small-scale features. As
239 an example, a 1024^3 grid dataset can be decomposed into nine resolutions/scales, where scale one
240 contains the coefficients with the smallest (finest) features and scale nine the largest (strongest)
241 features. In the scenario where few users are present, only the missing decomposition scales will
242 be streamed to improve the data quality rather than having to resample the entire dataset again at a
243 resolution closer to the original. Including all scales will result in a lossless reconstruction of the
244 original dataset. This thresholding scheme is tested in Sections 5.1 , 5.2 and 5.3.

245 The second approach to coefficient selection is the isolation of specific bands, opposed to the
246 accumulation, in order to extract structures that may exist in specific scales. This analysis-based
247 approach that isolates structures by selecting specific scales is explored in Section 5.5. When co-
248 efficients are requested at a specific scale, all coefficients excluding the pure lowpass subset are
249 computed and transmitted to the user through the web services or visualization nodes. The advan-
250 tage of using this method for scale-based analysis is the added capability of detecting features that
251 might not exist in other scales.

252 The third and more costly thresholding method sorts all wavelet coefficients by magnitude. A
253 percentage of this ordered set of coefficients can be requested by the user for a reconstruction.
254 Coherent and incoherent feature extraction is also possible through this method and is discussed
255 in [1, 16]. A parallel implementation of the quick sort sorting algorithm was added to the GSL to
256 allow this type of analysis.

257 A companion reconstruction framework is made available to the analysis node in order to cor-
258 rectly refine additional coefficients for data visualization. In practice, reconstruction is not required
259 on the visualization node, further reducing the latency. With their spatial coherence to the data, co-
260 efficients themselves can be visualized after a simple scaling operation. Data reduction is achieved
261 by utilizing subsets of coefficients smaller than the size of a full-resolution dataset. Bandwidth and
262 compute are therefore reduced between the communication pipeline of the database cluster and vi-
263 sualization node allowing the node to exist outside of the cluster.

264 When a user makes a request to the database cluster, coefficients not in cache or stored already
265 are computed through an on-the-fly data decomposition. After being cached, the coefficients are
266 transmitted to the visualization node where they are used to perform reconstruction on-the-fly if
267 refinement is needed or used directly for visualization.

268 4.2. Visualization Node

269 The primary visualization tool used in this node is Paraview [26]. Paraview is an open source
270 visualization software that can be adapted to many architectures and visualization applications.
271 The extensive feature list Paraview provides, including visualization and analysis tools, makes it
272 an ideal companion for a large database cluster.

273 Modifications were made to the Paraview source to allow communication with the JHTDB
274 to access both raw data or derived wavelet coefficients from the cluster. Natively, the tool does
275 not support data-level wavelet compression, therefore, our heavily customized GSL was adapted
276 to provide Paraview with full support. The purpose of data-level compression is to significantly
277 reduce the cost of analysis for large datasets while preserving relevant features and allowing a
278 large number of concurrent users per visualization node. As an example, a full resolution 1024^3
279 grid at floating-point precision can consume a minimum of 4 gigabytes (GB) of RAM for a simple

280 full-scale analysis. By using wavelet compression at the first scale, the memory requirement can
281 be directly reduced by 1/8th in size without significant loss of fidelity. On a commodity-based
282 visualization node with 64GB of RAM, a 10 concurrent-user scenario can immediately be turned
283 into one supporting 100+ concurrent users, and beyond with additional compression.

284 The data analysis tools provided by Paraview also expand the computational capabilities of
285 the JHTDB. A framework for user-driven analysis removes the restriction of only conforming to
286 the functions provided by the database cluster. Instead, a user can use a large set of mathematical
287 operators through Paraview to manipulate data remotely.

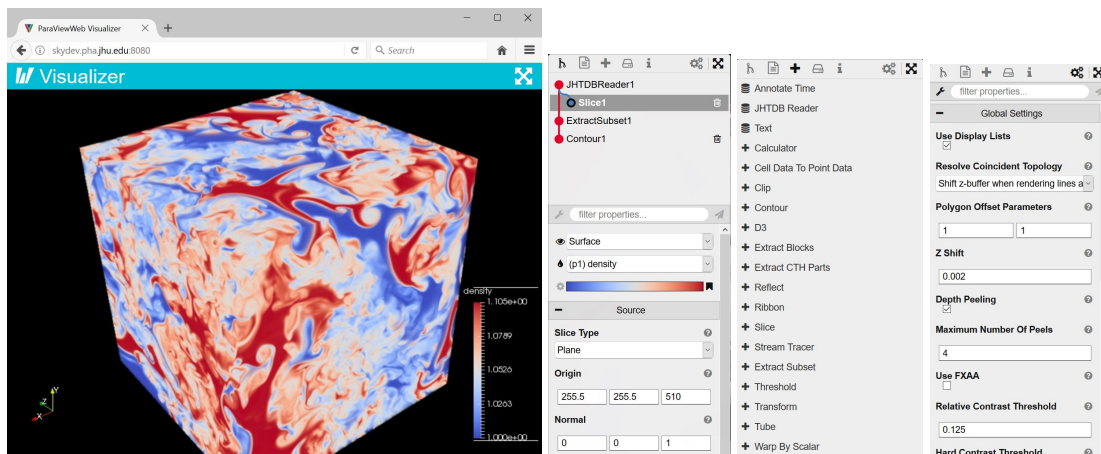


Figure 3: Remote visualization web interface (left) and sample UI elements (center,right). A sample view of the Paraview Web interface shows how many of the core paraview features are made available over the web. As an example, a large turbulence dataset (left) can be volume visualized and made viewable on any light-weight web-browser client.

288 Besides its analysis tools, Paraview provides several remote visualization capabilities through a
289 direct client-server connection or a web interface. The web module (Paraview Web) allows remote
290 users to access database datasets through a web browser in real-time. Paraview has compression
291 capabilities already implemented at the image rendering level as well as some support for geometry
292 processing [14]. Thus, it is possible to render data on the server itself and transmit a lower-quality
293 image to a user in low-bandwidth remote settings. Interactive rendering framerates between a
294 user's local web client and the remote visualization server are mainly limited by their physical

295 distance, impacting round-trip time over the Internet. If a dataset is small enough, with wavelet
296 compression enabled, geometry data needed to render iso-surfaces, for example, can be transmitted
297 directly to a remote user. Geometry can be rendered locally in our web client with a modern web
298 browser that supports WebGL for higher framerates. As seen in Fig. 3, we support an interface
299 that is similar to that of a standard Paraview desktop interface. A subset of the most frequently
300 used Paraview tools that can be generalized to most datasets is available over the web, reducing
301 time and resources needed to analyze and visualize large datasets in spatial and temporal space.
302 We view the following operators as the most commonly used: Calculator, Contour, Clip, Slice,
303 Volume, Threshold, Extract subset, Glyph, and Stream tracer.

304 Our web interface significantly reduces the overall effort required to perform large-scale data
305 analysis when no additional software must be installed by a user. This also reduces the entry
306 compute cost for performing data analysis since light-weight mobile devices may also be used.
307 The design trade-off for remote rendering versus sending entire datasets to a local client becomes
308 even more significant as much larger datasets (4096^3) are planned to be made available for the
309 JHTDB.

310 **5. Tests and Discussion**

311 In this section we provide results when benchmarking the architectural improvements pre-
312 sented in this paper with two datasets available in the database cluster. All datasets are split
313 spatially between eight database nodes and a single visualization node is used. The first dataset
314 is a DNS of homogeneous buoyancy driven turbulence (HBDT) [2]. The second dataset is a DNS
315 of forced magnetohydrodynamic turbulence (FMHDT) [3]. Both datasets consist of 1024 files
316 corresponding to different time instances. Each file stores density, three velocity components,
317 and pressure for the first dataset and three velocity components, pressure, three magnetic field
318 and magnetic vector potential components for the second dataset at 1024^3 grid points. Efficiency
319 is determined for computation overhead, bandwidth savings, and total latency from a complete
320 analysis pipeline for single and multiple time steps. Quality is examined for different scales and
321 resolution levels. Finally, we provide an example of scale-based analysis through the use of the
322 added wavelet framework.

323 *5.1. Efficiency*

324 We have also performed a series of benchmarks for a scenario where a single 1024^3 dataset
325 is accessed and visualized by a single user at multiple scales. The visualization node hardware
326 consists of a dual-socket, Intel Xeon E5440 at 2.83 GHz with 32GB of system RAM. The node
327 is headless and does not have a GPU, therefore rendering is done on the CPU using Windows'
328 Advanced Rasterization Platform included with Windows Server Datacenter edition.

329 Our benchmark simulates a scenario where data are decomposed by the database compute
330 module on-the-fly, cached, and reconstructed if necessary on a visualization node. This bench-
331 mark executes a fixed analysis pipeline that generates volume and isosurface visualizations. These
332 isosurfaces are computed at the mean of the data range. As of result, the number of possible
333 concurrent users can be estimated by both time and memory requirements.

334 Fig 4 contains performance timings and memory usage metrics of the execution of this analysis
335 pipeline on an original quality DNS dataset (HBDT) and at reduced resolution using wavelets.
336 Compute times are based on an average of 3 runs. Visualization times are based on a single
337 threaded versions of the framework with no GPU, where 1 thread is used per user.

338 Each decomposed scale is represented by the spatial size of the coarse coefficients to the power
339 of 3. The scales considered here range from scale 1 using 512^3 coefficients (finest) to scale 3
340 using 128^3 coefficients (coarsest) and beyond. These sizes are indicative of the amount of data
341 manipulation that has to be done during analysis. Data retrieval times are measured considering
342 the initial (cache-miss) request for a dataset. A wavelet decomposition is measured by first being
343 computed on the full scale data and only served up to the requested level. As a caching step,
344 we store the data as its scale 2 coefficient state as seen in Fig. 4. To compute scale 3, we can
345 decompose the data down one level incurring a small compute cost or if scale 1, we can reconstruct
346 the coefficients up one level.

347 As observed, data retrieval times differ significantly due to the varying sizes of compression
348 levels and number of coefficients. During the initial scales of a wavelet decomposition, compute
349 times are relatively larger due to the large amount of fine coefficients computed. Additional levels
350 are subsequently computed much quicker as data are recursively reduced. Although decomposition
351 times are significant when computing coefficients on-the-fly, the total time is still less, nearly

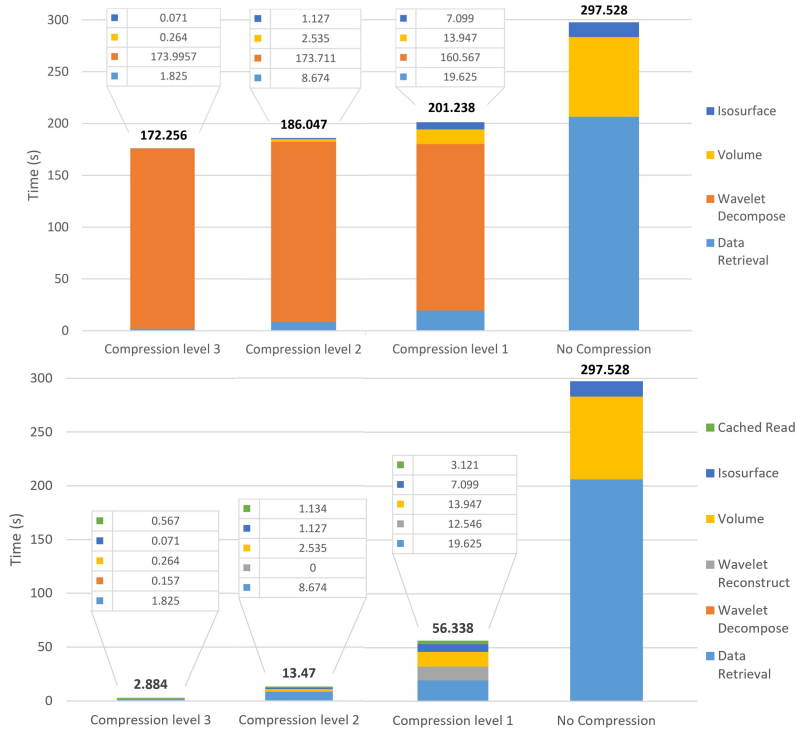


Figure 4: Benchmark. Intermediate and total time spent from request to visualization of a full resolution, 1024^3 dataset. Wavelet decomposition is performed on-the-fly before any caching is done (top) and once cached, only coefficients are served (bottom).

352 matching the data retrieval time of an entire dataset alone. By enabling compression, there still
 353 exists a net decrease in latency from initial query to final image. By reducing the amount of spatial
 354 data to process, the performance of downstream analysis operators significantly increases.

355 Unfortunately, due to storage limitations, a separate database of wavelet coefficients cannot
 356 be made available in parallel with the existing raw data. In the ideal case, a database of wavelet
 357 coefficients at all scales equal in size with the current datasets could enable minimal times for
 358 the features presented in this work. As compression still provides other benefits, we compute
 359 coefficients on-the-fly and use limited local storage as cache.

360 A data analysis pipeline can put significant burden on a system depending on the size of the
 361 dataset. As seen in Fig. 5, when considering the visualization pipeline, a high temporary memory

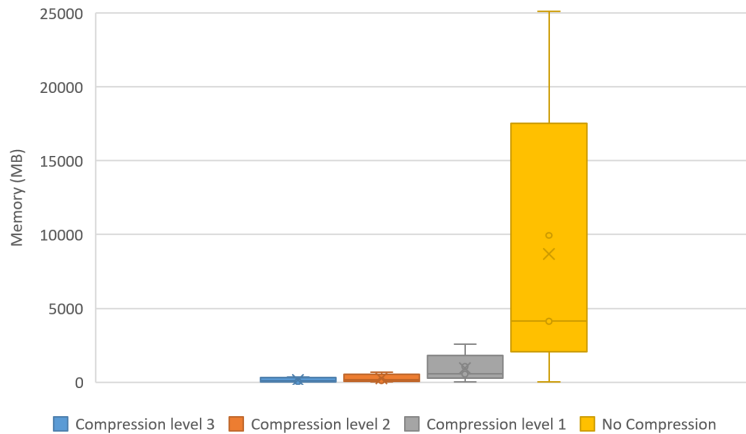


Figure 5: Memory Benchmark. Usage on the visualization node performing an analysis pipeline for a 1024^3 dataset. Analysis is done at several compression levels.

362 requirement was observed when computing isosurfaces and increased with the size of the dataset.
 363 During the isosurface computation for a 1024^3 data frame, the amount of RAM neared the 32GB
 364 virtual limit for the visualization node. If surpassed, this may cause the analysis node to incur a
 365 very high time penalty cost as the system would need to swap data out of RAM to the hard disk.
 366 The benefits of data analysis on spatially smaller representations of the data are both a reduction
 367 in compute cost and memory requirements, those of which significantly impact the total time to
 368 perform this analysis pipeline.

369 As more scales are requested, the wavelet machinery must perform more steps and decompose
 370 the data further, therefore increasing the decomposition compute cost. In addition to the reduced
 371 total compute cost, a larger amount of concurrent users can be supported as a direct result of cubic
 372 B-spline wavelet compression. Based on maximums in Fig. 5, a memory-bound node to 32GB
 373 can support many concurrent users: <200 users at level 3, <75 users at level 2, <14 users at level
 374 1, and a single user with no compression.

375 Further improvements are made by storing coefficient representations of the original data,
 376 effectively nullifying the on-the-fly wavelet decomposition computation time. The result of this
 377 implementation can reduce the total request time down to 2.9 seconds if we consider a Scale 3
 378 visualization of the data. Overall, the small initial cost of computing wavelet coefficients can be

379 greatly offset by the time saved during the transmission and analysis phase of the dataset. By
380 incorporating wavelets, inexpensive commodity hardware can be used to augment the turbulence
381 database cluster.

382 5.2. *Quality*

383 Performing wavelet compression up to certain scales does not always incur obvious costs in
384 quality. When a dataset is reconstructed up to a certain scale, the coefficients used for the recon-
385 struction include those below it. As an example, reconstructing scale 3 will also include those
386 in 4, 5,..., N th scale where N is the largest (coarsest) scale possible. Peak signal-to-noise ratio
387 (PSNR) is compared for various scales in Fig. 6 and Mean square error (MSE) in Fig. 7. As
388 expected, the inclusion of more scales produces more accurate representations for each dataset.
389 Primary quantities such as density and horizontal magnetic field are more sensitive to truncation
390 errors over the whole range of scales, while the reconstruction quality for derived quantities, such
391 as vorticity, stays relatively constant over the intermediate scales. This is expected since derived
392 quantities depend more on the small scales. Nevertheless, the error levels are relatively small for
393 all these quantities beyond scale 3. The compact support of cubic B-spline wavelets and thus,
394 strong localization properties, allows them to represent turbulence data relatively accurately with
395 a significantly reduced number of coefficients.

396 A qualitative analysis is performed on a subset of the compressed field using a volume visu-
397 alization in Fig. 8. The first scale in compression shows very little changes to the HBDT scalar
398 density field. At the initial scale, flow characteristics are preserved well at the data level and visual
399 fidelity is hardly affected. A more pronounced effect begins to form after the second compression
400 scale where oscillations start to form around the selected structure. This scale already represents
401 a 1/64th resolution size of the original. While the third scale represents a very large reduction in
402 size, overall features are still preserved but oscillations near the edges begin to intensify.

403 The preservation of smooth surfaces and localized features becomes important for preserving
404 derivatives quantities. These characteristics are explored with comparisons of derived isosurfaces
405 in Fig. 9. As with the previous analysis on the HBDT scalar density field, the first two compression
406 scales preserve the overall smoothness and local features of turbulence data. Beyond Scale 3, the

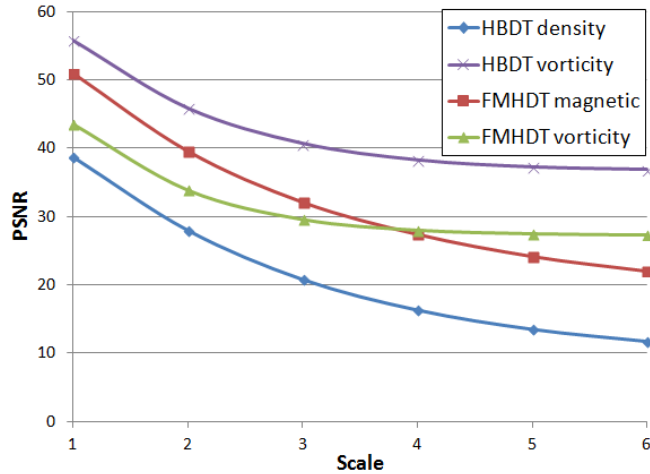


Figure 6: PSNR up-to each scale. Higher values are better.

407 preservation of interactions between small, localized features can no longer be guaranteed and
 408 data artifacts such as ripples begin to appear along isosurfaces. Alternatively, in some turbulence
 409 applications the interactions between large-scale features are of interest. For this type of analysis,
 410 the large-scale interactions inside the compressed flow are still well represented with even coarser
 411 decompositions than Scale 3.

412 5.3. Temporal Analysis

413 A direct benefit of integrating our wavelet framework with a database is the reduction in effort
 414 to perform temporal analysis. Although neither HBDT nor FMHDT datasets are spatially very
 415 large at a grid resolution of 1024^3 compared to the largest simulations performed to date, they
 416 span a time interval represented by at least 1000 time frames. A temporal benchmark has been
 417 performed on a shared resources server visualizing 60 time steps of a 512^3 HBDT density subset.
 418 As seen in Fig. 10, the summation of each time step includes the cost of requesting a new dataset
 419 from the database, wavelet decomposition and reconstruction (for Scale 2), and volume visualiza-
 420 tion. In addition, cached benchmarks for both datasets are available by using the databases native
 421 caching functionality. As observed, there is a significant improvement in latency when considering
 422 a cached version of the data, but more importantly a compressed Scale 2 equivalent of a dataset.

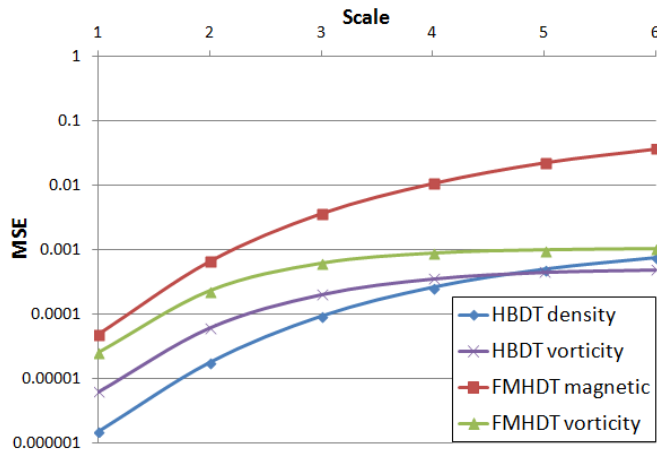


Figure 7: MSE up-to each scale. Lower values are better.

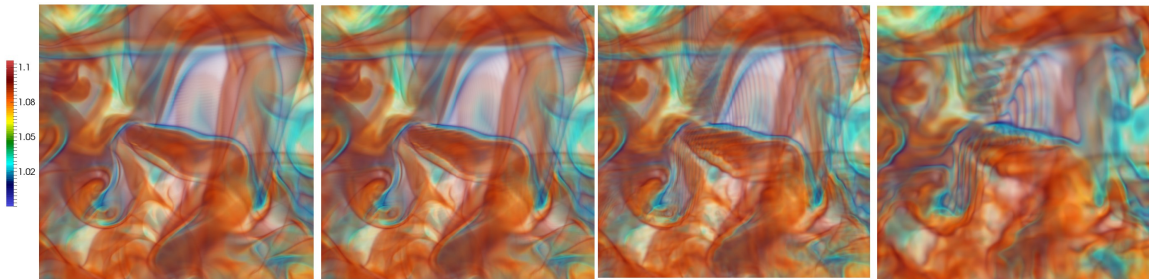


Figure 8: Volume visualization of HBDT density. A close-up of a feature to show the compression characteristics of cubic B-spline wavelets at each data level. From left to right: original, scale 1, scale 2, scale 3. Visible differences are minimal between the original and scale 1. Scale 2 begins to exhibit lossy features and by scale 3, most of the features begin to lose their finer structures around the edges.

423 The summation of time to visualize 60 time steps is 3024 secs (1370 secs cached) for the non-
 424 compressed data, and 1019 secs (191 secs cached) for a Scale 2 compression. The visualization
 425 results can be seen in Fig. 11. Qualitatively, HBDT volume density can be visualized at a reduced
 426 scale with no significant compromise on the final visualization.

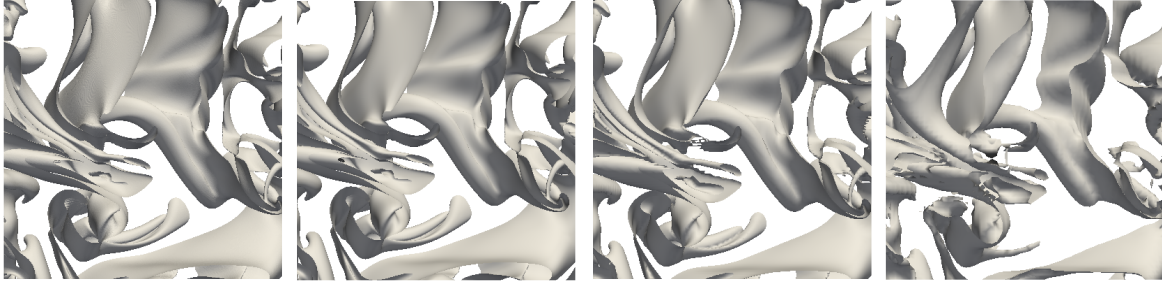


Figure 9: Isosurface visualization of HBDT density. A close-up of a feature to show the compression characteristics of cubic B-spline wavelets at the data level. From left to right: original, scale 1, scale 2, scale 3. Structures are generally well preserved up to Scale 2, where lossy features begin to appear. At scale 3, most of the features begin to lose their finer structures around the edges of isosurfaces appearing as artifacts.

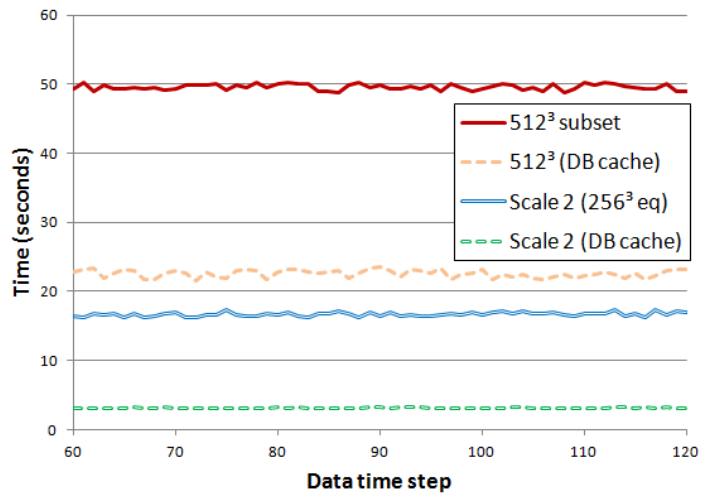


Figure 10: Temporal visualization benchmark. Volume visualization for 60 timesteps was performed for a 512^3 subset, and a Scale 2 (256^3 equivalent) wavelet. Total visualization times are 3024s (1370s cached) for non-compressed, and 1019s (191s cached) for Scale 2 compression.

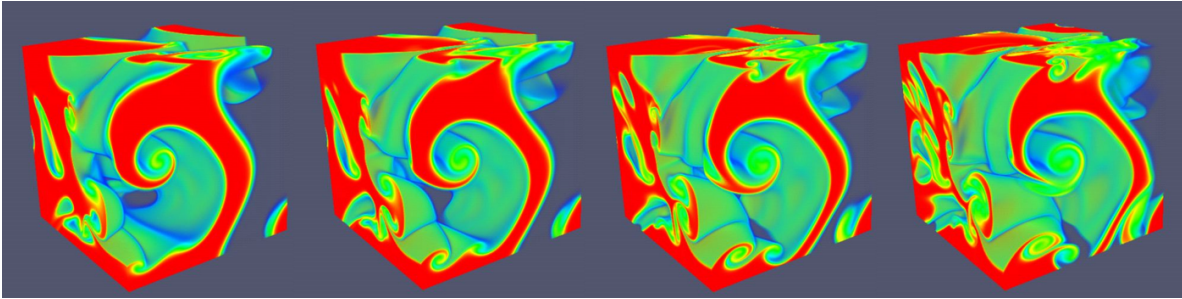


Figure 11: Temporal volume visualization of HBDT density. Wavelet integration and caching capabilities make it possible to quickly visualize multiple datasets to improve temporal understanding of a turbulence dataset. These four time steps represent frames 60,75,90,105 out of the 1024 total frames.

427 5.4. Scale-based Wavelet Analysis

428 This section provides an example of scale-based analysis through the use of the added wavelet
 429 framework. Scales are extracted from a dataset by isolating the coefficients extracted in each
 430 individual decomposition step. Compared to the previous section where we preserve coefficients
 431 up-to a specific scale, this section involves looking at each scale individually.

432 Fig. 12 shows the two datasets with two basic quantities specific to each dataset decomposed
 433 into several scales. Each scale contains amounts of positive (red) and negative (blue) quantity cap-
 434 tured per scale, where the sum of all individual scales results in the original. Three-dimensional
 435 turbulence is a strongly multi-scale phenomenon, with local and non-local interactions among the
 436 various scales. When the range of scales is large enough, which is the case with most practi-
 437 cal flows, the energy is transferred from the energetic large scales (where the energy is usually
 438 deposited) to the smallest scales (where the energy is usually dissipated).

439 This "cascade" of energy paradigm involves a hierarchy of vortex sizes and structure shapes.
 440 Unfortunately, the usual decompositions in Fourier space are non-local in physical space and spe-
 441 cific physical structures can not be easily associated with certain scales.

442 5.5. Significance of wavelet analysis

443 Multi-resolution geometric representation methods have emerged as more appropriate tools
 444 for scale decomposition and better connection with flow features. For example, using the curvelet

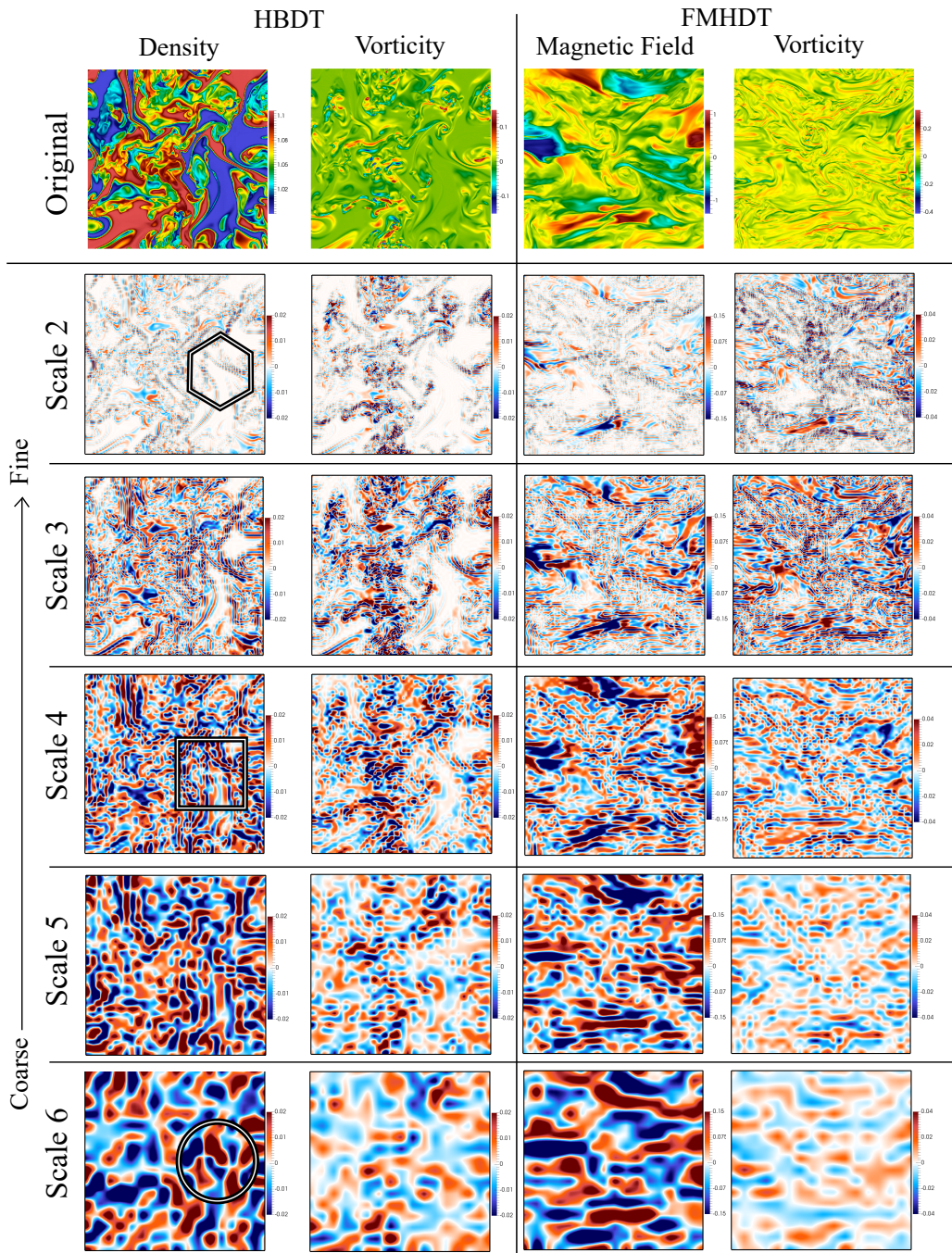


Figure 12: Turbulence visualization by scale. Homogeneous Buoyancy Driven Turbulence (Left) and Forced Magneto-Hydrodynamic turbulence (Right) are decomposed into several scales exhibiting multi-scale phenomena. Globular (blob) structures can be observed at the coarser (higher) scales (circles), while tube structures (squares) and sheet-like structures (hexagons) emerge out of finer scales. By adding all scales, the original dataset can be reconstructed losslessly.

445 transform, [27] [28] have shown a geometrical progression from blobs through tubes to sheet-like
446 structures with decreasing physical scale in a simple forced turbulence flow. Such knowledge can
447 be useful to understand and characterize the cascade process and also to inform physics-based
448 subgrid models used in affordable coarse mesh computations.

449 The flows exemplified here are more complex than those used in the past for this type of anal-
450 ysis. In addition, to demonstrate the remote analysis of large datasets, we are using B-splines
451 wavelets, which have been scarcely used before for such analyses, but can have distinct advan-
452 tages [1].

453 The HBDT flow represents the mixing between initially segregated fluids with different den-
454 sities as they start moving under the influence of gravity (or external acceleration). The fluids are
455 initially at rest and organized in pure-fluid random patches. As the buoyancy force starts mov-
456 ing the two fluids, the velocities increase in magnitude, while hydrodynamic instabilities, such as
457 Kelvin-Helmholtz instability, start to generate vortical motions at the interfaces between the fluid
458 patches. Thus, unlike previous applications of multi-resolution representation methods where the
459 scalars were passively advected by the velocity field, in this case the density represents an active
460 scalar, which feeds back into the velocity evolution. The full field showed in Fig. 12, first col-
461 umn, top, is taken at the time when significant mixing and vorticity generation has already been
462 produced, while both light (blue) and heavy (red) pure fluids are still present. Moving downwards
463 along the first column in Fig. 12, one can look at the density field structure from small to large
464 scales

465 At the level of the largest scales, the density exhibits a globular (blob) structure, with no
466 specific orientation bias. However, at the next two finer scales, the physical structure shows the
467 emergence of tubes preferentially oriented in the direction of gravity. As the scales become finer,
468 the tubes also become narrower and lose the vertical orientation. Finally, at the smallest scales, the
469 tubes are almost completely vanished and replaced with sheet-like structures. However, unlike the
470 passive scale case studied before, these structures are more difficult to identify, as globular (blob)
471 structures are still present and dominate the range of values shown in the legend. While the general
472 picture encountered before in the passive scalar case of blobs to tubes and to sheets is still present
473 approximately, we note that the presence of blobs at the finest scale is consistent with the mixing

474 asymmetry identified in the variable density case, with the pure heavy fluid mixing slower than
475 the pure light fluid [29, 30, 31]. Thus, these results show that the current subgrid models based
476 on passive scalar considerations need to be revisited for variable density flows to account for the
477 presence of unmixed (or less mixed) fluid blob structures down to the smallest scales.

478 A relatively different behavior is observed in the scale decomposition of the horizontal vorticity
479 for the HBDT flow. Since the vorticity is primarily generated at the interface between the fluid
480 blobs by fluid instabilities, there is a good correlation between density and vortical fields in the
481 full signal. Nevertheless, the tube like structure is less apparent at intermediate scales, as well as
482 alignment with horizontal or vertical directions. The alignment is mostly with the interfaces of the
483 fluid patches. This, again, makes modeling of such a flow more complicated, since the subgrid
484 models for the velocity field need to account for the structure of the active scalar (density) field.

485 The FMHDT flow [3], is also more complicated than previous attempts to characterize turbu-
486 lence using multi-resolution representation methods. In this case, again, there is a full feed-back
487 between the velocity and magnetic fields. Using the previous representation, we decompose the
488 horizontal magnetic field seen as an active scalar. At large and intermediate scales, there is a good
489 correlation between the vorticity and magnetic fields which tend to consist of structures elongated
490 in the x-direction. These structures become narrower and sheet-like at smaller scales, where most
491 of the correlation between the two fields is no longer present. However, even at the smallest
492 scales, there are regions of intense vorticity and magnetic field which are relatively well correlated
493 between the two fields, while the rest of the structures remain poorly correlated. Again, this under-
494 lies the difficulty in understanding the cascade process and constructing subgrid models for such
495 strongly coupled flows.

496 **6. Conclusion**

497 We have introduced a new, improved system architecture for a public database cluster of large
498 turbulence datasets. Until recently, the visualization and analysis of such datasets has been re-
499 stricted to a few groups worldwide with access to large supercomputers. The public Johns Hop-
500 kins Turbulence database (JHTDB) simplifies the access to multi-Terabyte turbulence datasets and
501 facilitates the computation of statistics and extraction of features through the use of commodity

502 hardware. Visualization support has been added for this database and wavelet analysis tools have
503 been implemented to expand the capabilities for this database cluster. Finally, wavelet compres-
504 sion has been introduced at the data-level to reduce access costs, reduce bandwidth and improve
505 latency between database components. This component also reduced the memory footprint of
506 datasets required for data analysis, effectively adding support for many concurrent users. The pa-
507 per demonstrates the new tools both for enabling remote visualization and turbulence data analysis
508 for two of the datasets hosted by JHTDB. These tools should help to extend the reach and analysis
509 power and ultimately the goals of such public databases.

510 For future work, we would like to move the visualization node away from the JHTDB and into
511 the cloud through Amazon Web Services (AWS). Currently, the user-interaction latency is limited
512 by the physical distance between a user and the location of the JHTDB. In this paper, We've re-
513 duced the amount of data needed to visualize so it may be feasible to make transfers external to
514 the visualization node from the database. Additionally, if we dynamically and transparently allo-
515 cate nodes for a user on AWS, and select a location that is physically the closest, user-interaction
516 latency would be significantly reduced.

517 **Acknowledgment**

518 The authors would like to thank LANL and Johns Hopkins University for supporting this work.
519 Los Alamos National Laboratory is operated by Los Alamos National Security, LLC for the US
520 Department of Energy NNSA under contract no. DE-AC52-06NA25396.

- 521 [1] J. Pulido, D. Livescu, J. Woodring, J. Ahrens, and B. Hamann. Survey and analysis of multiresolution methods
522 for turbulence data. *Computers and Fluids*, 125:39 – 58, 2016.
- 523 [2] D. Livescu, C. Canada, K. Kanov, R. Burns, IDIES, and J. Pulido. Homogeneous buoyancy driven turbulence
524 data set, 2014. <http://turbulence.pha.jhu.edu/docs/README-HBDT.pdf>.
- 525 [3] H. Aluie, G. Eyink, E. Vishniac, S. Chen, K. Kanov, R. Burns, C. Meneveau, and A. Szalay. Forced mhd
526 turbulence data set, 2013. <http://turbulence.pha.jhu.edu/docs/README-MHD.pdf>.
- 527 [4] E. Perlman, R. Burns, Y. Li, and C. Meneveau. Data exploration of turbulence simulations using a database
528 cluster. In *Proceedings of the ACM/IEEE Conference on Supercomputing*, 2007.
- 529 [5] Aaron Trott, Robert Moorhead, and John McGinley. Wavelets applied to loseless compression and progressive

- 530 transmission of floating point data in 3-d curvilinear grids. In *Proceedings of the 7th Conference on Visualization*
531 '96, VIS '96, pages 385–ff., Los Alamitos, CA, USA, 1996. IEEE Computer Society Press.
- 532 [6] Lars Lippert, Markus H. Gross, and Christian Kurmann. Compression domain volume rendering for distributed
533 environments. In *Computer Graphics Forum*, volume 16. Wiley Online Library, 1997.
- 534 [7] S. Guthe, M. Wand, J. Gonser, and W. Strasser. Interactive rendering of large volume data sets. In *IEEE*
535 *Visualization, 2002. VIS 2002.*, pages 53–60, Nov 2002.
- 536 [8] J. Woodring, S. Mniszewski, C. Brislawn, D. DeMarle, and J. Ahrens. Revisiting wavelet compression for
537 large-scale climate data using jpeg 2000 and ensuring data precision. In *Symposium on Large Data Analysis and*
538 *Visualization (LDAV)*, pages 31–38. IEEE, 2011.
- 539 [9] Sriram Lakshminarasimhan, Neil Shah, Stephane Ethier, Scott Klasky, Rob Latham, Rob Ross, and Nagiza F.
540 Samatova. *Compressing the Incompressible with ISABELA: In-situ Reduction of Spatio-temporal Data*, pages
541 366–379. Springer Berlin Heidelberg, Berlin, Heidelberg, 2011.
- 542 [10] P. Lindstrom. Fixed-rate compressed floating-point arrays. *IEEE Transactions on Visualization and Computer*
543 *Graphics*, 20(12):2674–2683, Dec 2014.
- 544 [11] James Ahrens, Berk Geveci, and Charles Law. Paraview: An end-user tool for large-data visualization. *The*
545 *Visualization Handbook*, page 717, 2005.
- 546 [12] Hank Childs, Eric S. Brugger, Kathleen S. Bonnell, Jeremy S. Meredith, Mark Miller, Brad J Whitlock, and
547 Nelson Max. A contract-based system for large data visualization. In *Proceedings of IEEE Visualization 2005*,
548 page 190–198, 2005.
- 549 [13] W. J. Schroeder, L. S. Avila, and W. Hoffman. Visualizing with vtk: a tutorial. *IEEE Computer Graphics and*
550 *Applications*, 20(5):20–27, Sep 2000.
- 551 [14] A. Cedilnik, B. Geveci, K. Moreland, J. Ahrens, and J. Favre. Remote large data visualization in the paraview
552 framework. In *Proceedings of the 6th Eurographics Conference on Parallel Graphics and Visualization, EGPGV*
553 '06, pages 163–170, 2006.
- 554 [15] M. Treib, K. Burger, F. Reichl, C. Meneveau, A. Szalay, and R. Westermann. Turbulence visualization at the
555 terascale on desktop pcs. *IEEE Transactions on Visualization and Computer Graphics*, 18(12):2169–2177, 2012.
- 556 [16] O. Roussel, K. Schneider, and M. Farge. Coherent vortex extraction in 3d homogeneous turbulence: comparison
557 between orthogonal and biorthogonal wavelet decompositions. *Journal of Turbulence*, page N11, 2005.
- 558 [17] D. Laney, P. t. Bremer, A. Mascarenhas, P. Miller, and V. Pascucci. Understanding the structure of the turbu-
559 lent mixing layer in hydrodynamic instabilities. *IEEE Transactions on Visualization and Computer Graphics*,
560 12(5):1053–1060, Sept 2006.
- 561 [18] P. T. Bremer, G. Weber, V. Pascucci, M. Day, and J. Bell. Analyzing and tracking burning structures in lean
562 premixed hydrogen flames. *IEEE Transactions on Visualization and Computer Graphics*, 16(2):248–260, March
563 2010.

- 564 [19] J. Graham, M. Lee, N. Malaya, R.D. Moser, G. Eyink, C. Meneveau, K. Kanov, R. Burns, and A. Szalay.
565 Turbulent channel flow data set, 2013.
- 566 [20] Y. Li, E. Perlman, M. Wan, Y. Yang, C. Meneveau, A. Burns, S. Chen, E. Szalay, and G. Eyink. A public
567 turbulence database cluster and applications to study lagrangian evolution of velocity increments in turbulence.
568 *Journal of Turbulence*, 9(31), 2008.
- 569 [21] I. Daubechies. Ten lectures on wavelets. *PA: SIAM*, 1992.
- 570 [22] M. Farge. Wavelet transforms and their applications to turbulence. *Annual Review of Fluid Mechanics*,
571 24(1):395–458, 1992.
- 572 [23] W. Sweldens. The lifting scheme: A construction of second generation wavelets, 1997.
- 573 [24] M. J. Shensa. The discrete wavelet transform: wedding the a trous and mallat algorithms. *IEEE Trans. on Signal*
574 *Processing*, 40(10):2464–2482, 1992.
- 575 [25] B. Gough. *GNU Scientific Library Reference Manual - Third Edition*. Network Theory Ltd., 3rd edition, 2009.
- 576 [26] U. Ayachit. *The ParaView Guide: A Parallel Visualization Application*. Kitware Inc., Clifton Park, NY, 2015.
- 577 [27] I. Bermejo-Moreno and D. I. Pullin. On the non-local geometry of turbulence, 2008.
- 578 [28] Y. Yang, D. I. Pullin, and I. Bermejo-Moreno. Multiscale geometric analysis of lagrangian structures in isotropic
579 turbulence, 2010.
- 580 [29] D. Livescu and J. R. Ristorcelli. Variable-density mixing in buoyancy-driven turbulence. *J. Fluid Mech.*,
581 605:145–180, 2008.
- 582 [30] D. Livescu and J. R. Ristorcelli. Mixing asymmetry in variable density turbulence. In *Advances in turbulence*
583 *XII*, pages 545–548. Springer, 2009.
- 584 [31] D. Livescu. Numerical simulations of two-fluid turbulent mixing at large density ratios and applications to the
585 RayleighTaylor instability. *Phil. Trans. R. Soc. A*, 371:20120185, 2013.